CANADIAN JOURNAL OF REMOTE SENSING
2017, VOL. 43, NO. 1, 28–47
http://dx.doi.org/10.1080/07038992.2017.1259556

Taylor & Francis
Taylor & Francis Group

Using Landsat Time-Series and LiDAR to Inform Aboveground Forest Biomass Baselines in Northern Minnesota, USA

Ram K. Deo[a], Matthew B. Russell[a], Grant M. Domke[b], Christopher W. Woodall[b], Michael J. Falkowski[c], and Warren B. Cohen[d]

[a]Department of Forest Resources, University of Minnesota, 1530 Cleveland Ave. North, St. Paul, MN 55108, USA; [b]Northern Research Station, Forest Inventory and Analysis, USDA Forest Service, 1992 Folwell Ave., St. Paul, MN 55108, USA; [c]Department of Ecosystem Science and Sustainability, Colorado State University, Fort Collins, CO 80583, USA; [d]Pacific Northwest Research Station, USDA Forest Service, 3200 SW Jefferson Way, Corvallis, OR 97331, USA

ABSTRACT

The publicly accessible archive of Landsat imagery and increasing regional-scale LiDAR acquisitions offer an opportunity to periodically estimate aboveground forest biomass (AGB) from 1990 to the present to align with the reporting needs of National Greenhouse Gas Inventories (NGHGIs). This study integrated Landsat time-series data, a state-wide LiDAR dataset, and a recent cycle of the national forest inventory (NFI) records in Minnesota, USA, to obtain a spatially explicit inventory of AGB across a large region of space and time back to the 1990 baseline used by the US NGHGI. Pixel-level polynomial models were fit to 6 time-series metrics of Landsat data to obtain fitted predictors that were ultimately coupled with the NFI data in a nonparametric modeling framework to map temporal AGB baselines. Eighteen candidate models, formulated using different combinations of LiDAR and Landsat metrics, revealed that the model using both Landsat and LiDAR metrics consistently performed better than the alternative models. The RMSE of the model using both Landsat and LiDAR was 27.2 Mg ha^{-1}, against 31.39 Mg ha^{-1} for the model using only LiDAR metrics. We conclude that the fitted Landsat-based model (RMSE = 47.64 Mg ha^{-1}) provides acceptable accuracy for the 1990-baseline mapping of AGB.

RÉSUMÉ

Les archives accessibles au public d'images Landsat et l'augmentation des acquisitions LiDAR à l'échelle régionale offrent l'opportunité d'évaluer périodiquement la biomasse forestière aérienne «aboveground forest biomass (AGB)»de 1990 jusqu'à nos jours pour répondre aux besoins de rapports des inventaires nationaux de gaz à effet de serre (NGHGIs). Cette étude a intégré des données de séries temporelles Landsat, un ensemble de données LiDAR couvrant l'État et une série récente provenant des archives de l'inventaire forestier national «national forest inventory (NFI)»du Minnesota, aux États-Unis, pour obtenir un inventaire spatialement explicite de la AGB sur un grand domaine spatiotemporel, depuis le référentiel de 1990 utilisé par le NGHGI des États-Unis. Les modèles polynomiaux au niveau du pixel ont été ajustés à 6 mesures de séries temporelles de données Landsat pour obtenir des prédicteurs ajustés qui ont finalement été couplés avec les données de le NFI dans un cadre de modélisation non paramétrique pour cartographier les référentiels temporels de la AGB. Dix-huit modèles candidats formulés en utilisant différentes combinaisons des mesures de LiDAR et Landsat ont révélé que le modèle utilisant à la fois des mesures de Landsat et LiDAR a toujours une meilleure performance que les autres modèles. La REQM «root mean square error (RMSE)» du modèle utilisant à la fois Landsat et LiDAR était de 27,2 Mg ha^{-1}, contre 31,39 Mg ha^{-1} pour le modèle utilisant seulement des mesures de LiDAR. Nous concluons que le modèle ajusté basé sur Landsat (RMSE = 47,64 Mg ha^{-1}) fournit une précision acceptable pour la cartographie du référentiel de 1990 de l'AGB.

ARTICLE HISTORY
Received 18 February 2016
Accepted 14 October 2016

Introduction

The net difference between carbon removals from the atmosphere by forest growth and emissions due to disturbances provides an estimate of net forest carbon flux. Because forests efficiently store atmospheric carbon and contain about 80% of all aboveground organic carbon (Houghton et al. 2009; Pan et al. 2013), mapping and monitoring aboveground forest biomass (AGB) over time has gained international recognition in policy and operational decisions, especially in the context of climate change mitigation (Nabuurs et al. 2007). The spatial and temporal patterns of AGB at national and regional scales are essential for strategic planning purposes such as the National Greenhouse Gas Inventory (NGHGI) reporting per the United Nations Framework Convention on

CONTACT Ram K. Deo rkdeo@umn.edu
Copyright © CASI

Climate Change (UNFCCC). In addition, high-resolution, spatially explicit periodic maps that include a baseline of AGB could serve as a means to implement operational forest management and evaluate carbon dynamics attributed to forest management and disturbances (Powell et al. 2010). Although conventional approaches dependent only on field measurements can provide robust estimates (Zhang and Ni-Meister 2014), they are costly and difficult to implement over large spatial and temporal scales. Further, estimates of uncertainty are more likely exacerbated when inconsistent field-sampling protocols are employed over a long time period (e.g., since 1990, the UNFCCC baseline year for NGHGI reporting).

Temporal quantification of AGB must follow a robust and consistent approach in order to accurately portray historic disturbance and recovery in the process of sustainable forest management and monitoring programs such as Reducing Emissions from Deforestation and Forest Degradation Plus (REDD+). A number of REDD+ interventions and NGHGIs require large-area 1990 baselines of forest biomass as a means to quantify changes in carbon stocks. However, large-scale spatial inventories in the past that lacked sufficient field samples are challenging without coupling temporal geoinformation from satellite imagery with recent forest inventory data collected consistently across the region in representative samples. Landsat data, especially the imagery of Thematic Mapper (TM) and successor sensors since 1984, have been the most commonly used means to extract spatiotemporal details of forest structure from local to global scales because of the freely accessible archive of data at a 30-m spatial resolution (Huang et al. 2010; Lu et al. 2012). The historic archive, continuous observations, and digital quality of Landsat data have resulted in advanced image processing platforms and algorithms to obtain consistent analysis-ready data and metrics free from noise such as clouds and shadows (Banskota et al. 2014; Roy et al. 2014). For example, a pixel-level spectral-trend analysis and model fit to annual time-series metrics of Landsat data of a preset quality standard can be used to obtain fitted metrics for any target year in the past when there was persistent cloud cover (e.g., Kennedy et al. 2010). Indeed, combining Landsat predictors with national forest inventory (NFI) data has been common in different parts of the world for strategic inventories (McRoberts 2012; Schroeder et al. 2008), but reliable estimation also requires that the field data be collected based on a consistent sampling protocol. For example, the NFI system in the United States adopted a nationally consistent field-sampling design in 1999, and results indicate that population estimates were inconsistent with the estimates based on the previous sampling design (Goeking 2015).

Remote sensing and geographic information systems (GIS) have long been used to support forest inventories. A wide range of modeling approaches employing single or multisensor, passive or active remotely sensed data such as Landsat and LiDAR, have been documented for spatial inventories of AGB (Gleason and Im 2011; Koch 2010). Although multispectral Landsat data are frequently used in forest inventories and assessments (Powell et al. 2014), the sensor suffers from signal saturation in high biomass areas or forests with complex stand structures (Huete et al. 2014; Schroeder et al. 2008). Active sensors such as LiDAR offer improved sensitivity to 3-dimensional forest structure, resulting in AGB estimates with increased accuracies. Previous studies have demonstrated that LiDAR-derived metrics are highly sensitive to structural attributes and their application can improve the cost efficiency of forest inventories compared to traditional approaches (Hudak et al. 2009; Hummel et al. 2011). At a time when regional-scale LiDAR acquisitions have received much attention because of efficiencies in characterizing terrestrial biophysical attributes such as topography (e.g., MnTOPO 2014), the integration of regional LiDAR datasets with Landsat time-series data could improve the accuracy of large-area, spatiotemporal mapping of AGB. Further, one-time LiDAR data could support projection modeling based on annual time-series Landsat data to inform forest biomass and carbon baselines (Pflugmacher et al. 2014).

The standard approach in remote-sensing-based assessments of AGB employs formulation of multivariate relationships between the response measured in a limited number of field sample plots and colocated spatial metrics of remotely sensed data. The commonly used methods to formulate the relationships include parametric regression and nonparametric *k*-nearest neighbor (*k*-NN) imputation of different types. However, parametric regressions suffer from limitations that arise from sensitivity of the models to influential observations, multicolinearity of predictors, and inherent assumptions about homoscedasticity and linearity (Hayashi et al. 2015). The *k*-NN imputation methods have been popular in strategic inventories worldwide since the 1990s because multiple responses can be predicted simultaneously (Tomppo 1991) and the algorithms are not bound to parametric assumptions (Brosofske et al. 2014). In *k*-NN imputation, a set of reference points with known values of response and predictor variables is used to obtain responses at target points (i.e., with known predictors only) as weighted averages of *k*-nearest neighbors (in the reference set) selected via similarity of spatial covariates of the target and reference points (McRoberts 2012; Franco-Lopez et al. 2001). There are different variants of *k*-NN but the random-forest (RF)-based *k*-NN (Crookston and Finley

2008) is popular and widely used in geospatial inventory models of forest attributes because the approach is robust to collinearity of predictors, it ranks the importance of predictors, it provides a measure of model accuracy through internal cross-validation, and generally it gives better predictions compared with other imputation methods (Latifi et al. 2010; Moser et al. 2016). The RF-*k*NN algorithm is guided by an ensemble of many classification and regression trees in which each tree is built from a bootstrap subsample of a reference dataset, and each node in the tree is split via the best predictor chosen from a random subset of all predictors (Liaw and Wiener 2002). The RF-based nearness is estimated as the proportion of all trees in the ensemble that associate a target point with a particular subset of k points in the reference set. The value of k is an important parameter in imputation modeling because it can affect precision and accuracy.

The general objective of this study was to formulate and evaluate AGB projection models based on the consistent NFI data from northern Minnesota, USA, combined with fitted metrics obtained from pixel-level curve fitting to a suite of annual time-series (1986–2011) metrics of Landsat TM data. The RF-*k*NN based projection models trained using a recent cycle (2007–2011) of the NFI data are intended to establish AGB baseline estimates back to 1990, per UNFCCC requirements. Because Minnesota acquired statewide LiDAR in 2011, we first evaluated the accuracy of only the Landsat-dependent projection model for 2011 against the model using both LiDAR and Landsat derived metrics for the same year. The Landsat-based projection model was also tested in the year 2000, using an extant map developed for the National Biomass and Carbon Dataset (NBCD) circa 2000 (Kellndorfer et al. 2013). An additional objective was to analyze the effect of the number of nearest neighbors (k) on the accuracy of model predictions.

Methods

Study area

The study area encompassed a single Landsat scene (WRS-2 path 27/row 27; 47.4° N, 92.5° W) in northeastern Minnesota, USA (Figure 1). The area ($\sim$ 21,308 km^2) is primarily composed of aspen-birch (*Populus-Betula*) and spruce-fir (*Picea-Abies*) forest types, with interspersed wetlands and agricultural lands (McRoberts 2009). This site was chosen by considering the availability of both Landsat time-series and LiDAR data and the large extent of forest cover (approximately 75%) characterized by mixtures of hardwood and conifer species in uneven-aged and naturally regenerated stands. The past 30 years (1981–2010) of climatic records in the region show that the mean annual precipitation and temperature in the area ranged from 68 cm–84 cm and 1°C–5°C, respectively (MN DNR 2013). The terrain elevation in the area varies between 170 m–635 m above sea level.

Landsat time-series data and derived metrics

We obtained a time-series (1986–2011) of near-anniversary date Landsat-5 TM imagery for the study area (Table 1) from the US Geological Survey (USGS) Climate Data Record (CDR; USGS 2015a). The selected imagery in the time series contained less than 5% cloud cover, and each image was acquired between mid-July and mid-September (i.e., peak growing season in the area) when consistent landscape conditions and phenology persist due to similar solar geometry. The time-series surface reflectance imagery and other higher-level data products in the CDR were acquired through bulk ordering via the Earth resources observation and science (EROS) center science processing architecture (ESPA) Interface (USGS 2015). We downloaded surface reflectance of individual bands (visible and infrared), some spectral indices (USGS 2016), and cloud masks for each image. The data were already terrain corrected (L1T) and radiometrically and atmospherically preprocessed and available at 30-m spatial resolution. Because some of the selected imagery in the time series contained narrow cloud and shadow patches (i.e., $<$ 5% cloud cover), we removed that noise by using cloud masks and substituting with clear imagery acquired in adjacent years (Table 1). Note that there were only 17 images in the 26 years (1986 to 2011) that met the image selection criteria and that data gaps as long as 3 years were created.

We selected 6 spatial predictors from the Landsat data for AGB modeling: Band 5 surface reflectance, Normalized Difference Vegetation Index (NDVI), normalized burn ratio (NBR), integrated forest z-score (IFZ), tasseled cap angle (TCA), and disturbance index (DI). Among these, Band 5, NDVI, and NBR were obtained directly from the CDR, but we derived IFZ, TCA, and DI metrics as described in Huang et al. (2010), Pflugmacher et al. (2014) and Healey et al. (2005), respectively (Table 2). We used these predictors to optimize accuracy and parsimony of the models because published works have reported varying sensitivity of these metrics to different forest types (Foody et al. 2003; Heiskanen 2006; Lu et al. 2012).

Shortwave infrared (SWIR) reflectance, spectral indices and other disturbance metrics obtained from Landsat data are widely used in biomass modeling (Cohen and Goward 2004; Zhang and Ni-Meister 2014). SWIR reflectance (particularly TM Band 5) normally displays a strong negative relationship with biomass (Lu 2006; Steininger 2000). Because green leaves strongly

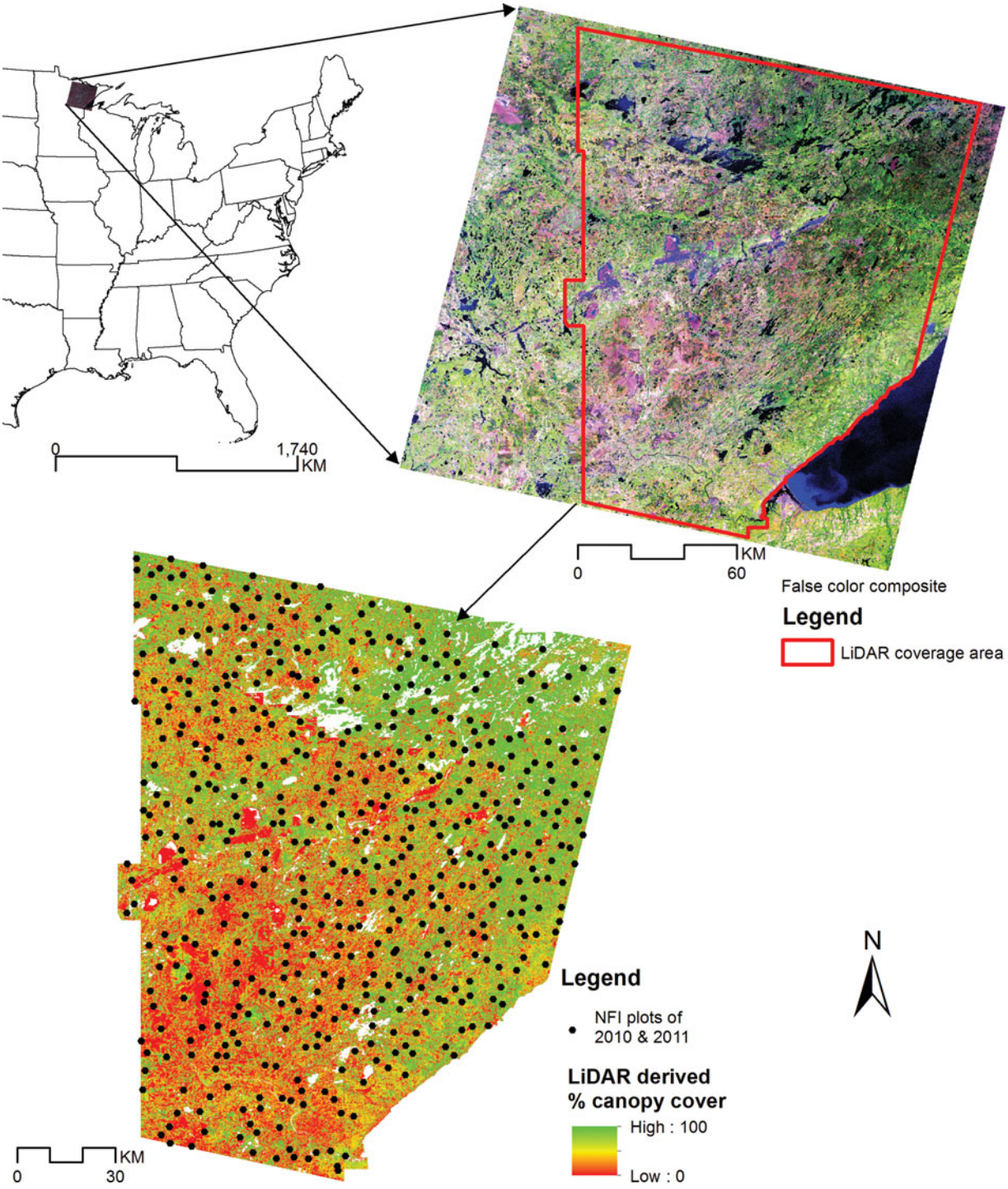

Figure 1. Study area in north-eastern Minnesota, U.S.A. The small rectangular grey area in the top-left figure represents the foot print of Landsat scene (WRS-2, path 27/ row 27) in Minnesota. The top-right figure is a false color composite (FCC) of the Landsat TM image captured on 11 September, 2011 with the bands 5, 4, and 1 displayed as red, green and blue, respectively. The red polygon inside the FCC represents the target area for which LiDAR dataset is also available. The pink-red and blue tones in the FCC represent open canopy areas and water bodies, respectively. The bottom figure represents LiDAR derived percentage canopy cover calculated based on all returns above 2-m ground level. The black dots represent the locations of NFI plots measured in 2010 and 2011 and the white patches are water bodies.

reflect in near-infrared and green wavelengths and absorb blue and red wavelengths from chlorophyll and leaf moisture, NDVI (i.e., the ratio of the difference and sum of reflectances in near-infrared and red bands) enhances vegetation signal (Huete et al. 2002; Lillesand et al. 2007). NDVI is preferred in global vegetation monitoring because the index is considered to signify green vegetation biomass. We included the NBR index because

Table 1. Time-series images for the Landsat scene (WRS-2 path 27/row 27) in northeastern Minnesota, USA.

Acquisition dates of target images	Julian day	Sun elevation	Cloud cover (%)	Dates of images (close to target) used to remove clouds/shadows
8/21/1986	233	47.36884545	0.1	8/24/1987; 6/30/1988
8/24/1987	236	47.17930498	1	8/21/1986; 6/30/1988
9/14/1989	257	40.6712713	0.1	7/29/1990; 8/10/1991
7/31/1990	212	52.10959186	0	—
9/6/1992	250	42.73507367	1	8/10/1991; 3/25/1993
7/29/1995	210	50.4158747	0.5	6/20/1996; 9/19/1994
9/4/1997	247	44.40180366	0.2	8/6/1998; 6/20/1996
8/6/1998	218	53.01775887	0.1	7/24/1999; 9/4/1997
7/24/1999	205	55.68874395	0	—
9/12/2000	256	42.33553749	0.1	7/24/1999; 8/14/1999
8/14/2001	226	51.2025708	5	6/30/2002; 9/12/2000
9/5/2003	248	44.73092109	0.1	6/30/2002; 8/6/2004
9/13/2006	256	43.40098642	0	—
9/16/2007	259	42.40882112	0.3	8/17/2008; 9/13/2006
8/17/2008	230	50.89746106	2.1	6/24/2009; 9/16/2007
8/23/2010	235	49.77087558	4	6/24/2009; 9/11/2011
9/11/2011	254	43.74637637	0.1	8/23/2010; 6/24/2009

it is reported to be correlated with field-measured burn severity indices and may characterize fire disturbances (Escuin et al. 2008). The IFZ metric, which is a measure of the likelihood of a pixel being forested, was considered because it provides a normalized predictor that can substantially reduce the spatial and temporal variability of spectral signatures caused by atmospheric conditions and sensor issues (Huang et al. 2010). It is reported that IFZ values are similar and low (<3) for deciduous and conifer forests in growing seasons and remain stable over time, but nonforest areas have high values. This characteristic of IFZ was thought to be useful to detect forest changes.

The TCA and DI metrics based on tasseled cap brightness (TCB), greenness (TCG), and wetness (TCW) indices (Crist and Cicone 1984) were used because a combination of more bands possibly contains more information than does an individual band. The tasseled cap indices, obtained as a linear combination of the 6 reflectance bands of TM, emphasize overall reflectance (brightness), contrast between near-infrared and visible reflectance (greenness), and contrast between visible/near-infrared and SWIR (wetness) (Crist and Cicone 1984). These indices are sensitive to phenological changes and have potential for revealing key forest attributes (Cohen and Goward 2004). Healey et al. (2005) found that tasseled cap indices and DI performed significantly better than TM bands reflectance in land cover change analysis; they also found that DI alone

Table 2. Spectral indices used in the spatial aboveground biomass models.

Index	Description
$\text{NDVI} = \frac{\text{Band 4} - \text{Band 3}}{\text{Band 4} + \text{Band 3}}$	Ratio of the difference and sum of near-infrared (TM Band 4) and red (TM Band 3) bands (USGS 2016)
$\text{NBR} = \frac{\text{Band 4} - \text{Band 7}}{\text{Band 4} + \text{Band 7}}$	Ratio of the difference and sum of near-infrared (TM Band 4) and second SWIR (TM Band 7) bands (USGS, 2016)
$\text{IFZ} = \sqrt{\frac{1}{3}\sum_{i=1}^{3}(\text{FZ}_i)^2}$ where $FZ_i = \frac{v_{pi} - \bar{v}_i}{SD_i}$	FZ_i is forest z-score of band i; v_{pi} is a pixel value and $\bar{v}_i$ and SD_i are mean and standard deviations of a sample of forested pixels. IFZ of a TM pixel is the integrated values of FZ_i for the Bands 3, 5, and 7 (Huang et al. 2010).
$\text{TCB} = 0.3037 \times \text{Band 1} + 0.2793 \times \text{Band 2} + 0.4743 \times \text{Band 3} + 0.5585 \times \text{Band 4} + 0.5082 \times \text{Band 5} + 0.1863 \times \text{Band 7}$	Tasseled cap brightness index for TM (Crist et al. 1984)
$\text{TCG} = -0.2848 \times \text{Band 1} - 0.2435 \times \text{Band 2} - 0.5436 \times \text{Band 3} + 0.7243 \times \text{Band 4} + 0.0840 \times \text{Band 5} - 0.1800 \times \text{Band 7}$	Tasseled cap greenness index for TM (Crist et al. 1984)
$\text{TCW} = 0.1509 \times \text{Band 1} + 0.1973 \times \text{Band 2} + 0.3279 \times \text{Band 3} + 0.3406 \times \text{Band 4} - 0.7112 \times \text{Band 5} - 0.4572 \times \text{Band 7}$	Tasseled cap wetness index for TM (Crist et al. 1984)
$\text{DI} = \text{B}_r - (\text{G}_r + \text{W}_r)$ where $\text{B}_r = (\text{TCB} - \text{B}_\mu)/\text{B}_\sigma$ $\text{G}_r = (\text{TCG} - \text{G}_\mu)/\text{G}_\sigma$ $\text{W}_r = (\text{TCW} - \text{W}_\mu)/\text{W}_\sigma$	B_r, G_r *and* W_r are rescaled tasseled cap brightness, greenness, and wetness indices, respectively; B_μ, G_μ and W_μ are average values of brightness, greenness, and wetness of samples of forested pixels; B_σ, G_σ and W_σ are standard deviations of brightness, greenness, and wetness of samples of forested pixels, respectively (Healey et al. 2005).
$\text{TCA} = \arctan(\text{TCG}/\text{TCB})$	Tasseled cap angle (Pflugmacher et al. 2012).

Table 3. Distribution of aboveground biomass (Mg ha^{-1}) across the national forest inventory plots in northeastern Minnesota, USA.

Inventory year	No. of plots	Min.	First quantile	Mean	Third quantile	Max.	Standard deviation
2000	262	0	32.06	75.55	111.88	266.35	55.96
2007	342	0	37.47	79.21	113.67	340.24	53.51
2008	340	0	35.54	76.59	111.87	260.61	53.01
2009	316	0	39.62	78.54	105.85	316.90	55.33
2010	336	0	30.63	78.11	110.99	318.64	59.00
2011	327	0	38.92	83.52	118.92	281.33	53.48

outperformed a combination of the tasseled cap indices or TM bands at some sites. DI is a linear combination of rescaled TCB, TCG, and TCW bands (Table 2) and it quantifies proximity of a pixel in tasseled cap space to the areas in the scene having the highest TCB and lowest TCG and TCW. TCW is found to be least affected by topographic variation in closed-canopy conifer stands and is more powerful than TCB and TCG for predicting forest structural attributes (Cohen and Goward 2004). As a substitute for TCW, Powell et al. (2010) and Pflugmacher et al. (2012) used TCA (i.e., arctan transformation of the ratio of TCG and TCB) that describes the gradient of percent vegetation cover within the TCB–TCG spectral plane.

LiDAR data and derived metrics

A LiDAR dataset with nominal pulse spacing of 1 m–1.5 m and vertical accuracy root mean square error (RMSE) of 5 cm is publicly available from the Minnesota Geospatial Information Office (MnGeo 2015a) for above 75% coverage of the target Landsat scene to the eastern side of the study region (Figure 1). The LiDAR data with multiple returns (up to 4) per pulse were acquired over a 24-day period in 55 flight missions in the spring of 2011 (May 3–26) primarily for the purpose of topographic mapping. The vendor, Woolpert, Inc., collected data using either a Leica ALS50 or Optec ALTM Gemini laser scanner onboard an aircraft at an average altitude of about 2,377 m above ground level, flying at an average ground speed of about 278 km hr^{-1}. The field of view (full), pulse rate, scan rate, and side lap (minimum) specifications of the LiDAR system were 40 degrees, 99 kHz, 38 Hz, and 25%, respectively. We obtained the raw LiDAR point-cloud data from the MnGeo web-portal (MnGeo 2015b) and processed them using FUSION software (McGaughey 2014) to generate 30 grid metrics representing canopy cover, canopy density, and vegetation height distribution at 30-m spatial resolution, following Falkowski et al. (2010) and Hudak et al. (2008). The target area for spatiotemporal inventory of AGB was limited to the aerial extent common to both the Landsat scene and the region of the LiDAR acquisition (i.e., about 75% of the Landsat scene, Figure 1).

National forest inventory data

The US Department of Agriculture (USDA) Forest Service started the nationally consistent annual forest inventory in Minnesota in 1999. The inventory design consists of permanent plots distributed over 5 panels in the entire state with an intensity of about 1 plot per 2,400 ha such that 1 panel is measured in a year and all plots are revisited on a 5-year cycle (Bechtold and Scott 2005). The plot layout consists of a cluster of 4 subplots with 1 central and 3 peripherals at 36.58-m (120-ft) horizontal distance and 0°, 120°, and 240° azimuths from the central subplot. Each subplot has a 7.32-m (24-ft) radius in which all trees 12.7 cm and greater in diameter at breast height (DBH) are measured for various dimensions, including DBH and total height. The tree size measurements were used in species-specific allometric models to obtain tree AGB, which were then aggregated to obtain plot-level estimates.

AGB data for the NFI plots measured in 2000 and 2007 to 2011 in the target area were obtained from the Forest Inventory and Analysis program at the Northern Research Station of the USDA Forest Service (Table 3). The plot biomass estimates, scaled to megagrams per hectare (Mg ha^{-1}), were based on the nationally consistent allometric models of Jenkins et al. (2003). These models are no longer used directly in the NFI program but were used in an extant AGB map production, circa 2000, for the National Biomass and Carbon Dataset (NBCD), which was used to evaluate the accuracy of stand-level AGB predictions in year 2000 based on models developed in this study. NBCD provides a high-resolution (30 m) spatially explicit map as a year-2000 baseline of AGB for the conterminous United States. Woods Hole Research Center[1] produced the NBCD map by integrating NFI plot data with the high-resolution Interferometric Synthetic Aperture Radar (InSAR) data acquired in the 2000 Shuttle Radar Topographic Mission and spectral data of Landsat Enhanced Thematic Mapper Plus (ETM+) acquired between 1999 and 2002 (Kellndorfer et al. 2013).

The NFI data from the recent inventory cycle (i.e., 2007 to 2011) were used for model training and the year

[1] http://whrc.org/

Table 4. Fitted RF-*k*NN models for aboveground biomass in northeastern Minnesota, USA.

Models	Predictors in the model[†]	[‡]Training data years	No. of plots	Values of *k*
TM_{fit5}	6 fitted Landsat metrics ($Band5_{fit}$; DI_{fit}; NBR_{fit}; IFZ_{fit}; TCA_{fit}; $NDVI_{fit}$)	2007 to 2011	1661	1; 3; 5
TM_{fit1}	6 fitted Landsat metrics ($Band5_{fit}$; DI_{fit}; NBR_{fit}; IFZ_{fit}; TCA_{fit}; $NDVI_{fit}$)	2011	327	1; 3; 5
$TM.LiDAR_{obs1}$	3 observed LiDAR metrics ($ElevMax_{obs}$; $CovAb2m_{obs}$; $ElevAv_{obs}$) and Landsat $Band5_{obs}$	2011	253	1; 3; 5
$LiDAR_{obs1}$	5 observed LiDAR metrics ($ElevMax_{obs}$; $ElevAv_{obs}$; $ElevAAD_{obs}$; $Stratum1_{obs}$; $Stratum5_{obs}$)	2011	253	1; 3; 5
TM_{obs4}	6 observed Landsat metrics ($Band5_{obs}$; DI_{obs}; NBR_{obs}; IFZ_{obs}; TCA_{obs}; $NDVI_{obs}$)	2007 to 2011, except 2009	1347	1; 3; 5
TM_{obs1}	6 observed Landsat metrics ($Band5_{obs}$; DI_{obs}; NBR_{obs}; IFZ_{obs}; TCA_{obs}; $NDVI_{obs}$)	2011	327	1; 3; 5

[†] ElevMax (elevations maximum), ElevAv (elevations average), CovAb2m (canopy cover based on proportion of all returns above 2 m), ElevAAD (elevations average absolute deviation), Stratum 1 (proportion of aboveground returns below1.5 m) and Stratum 5 (proportion of vegetation returns above 10 m and below 20 m) are LiDAR-derived observed metrics.
[‡] The plot-level predictors and AGB data in the model frame matched temporally.

2000 data were used for model validation. The distribution of AGB per plot for the pooled dataset is given in Table 3. Six different AGB models (Table 4) and corresponding maps were developed in 2011 because the LiDAR data acquired in that year was expected to produce the strongest predictors for modeling. After evaluating the performance of only Landsat-dependent models against LiDAR-dependent models in 2011, we extended the most suitable Landsat-dependent model to produce spatially explicit AGB maps for the years 1990, 1995, 2000, 2005, 2010, and 2011 so that we would have a baseline (1990) estimate and a product for comparison with the reference NBCD (2000) map. We avoided production of yearly maps to minimize the modeling time.

Modeling and evaluation approach

Because obtaining cloud-free Landsat imagery at nominal intervals for the entire study area is unlikely, a pixel-level polynomial (3rd-degree) curve fit tool (De Jager and Fox 2013) was applied to each of the 6 time-series predictors obtained from the Landsat time-series data (i.e., 17 images from 1986 to 2011, Table 1). The 3rd-degree polynomial curve fitting was assumed to better represent the temporal spectral trend than the 1st- and 2nd-degree polynomials, following Lawrence and Ripple (1999). The assumption was justified from a linear regression analysis wherein we fit the 1st-, 2nd- and 3rd-order polynomials to cluster means of each TCB band in the time series. The time-series TCB bands were subject to unsupervised clustering (via the Iso Cluster tool in ArcGIS) into 20 arbitrary classes, and polynomial models were fit to each class with the cluster mean TCB as the response and the cumulative number of growing seasons since the first image date (1986) as the explanatory variables (e.g., Lawrence and Ripple 1999). Of the 20 curve fits, the majority (16) were found to favor the 3rd-degree polynomial. This was determined via a stepwise (both direction) model selection procedure based on the Akaike information criterion (AIC), which we implemented in the R statistical software (R Core Team 2015). We drew a similar inference when average values of TCB in small polygons (about 500 pixels) at 20 forested locations of varying percent canopy cover were analyzed in the time series via polynomial fit. Isoclustering of NDVI and Band 5 and its temporal fit also revealed superior performance of the 3rd-degree polynomial. Because some studies have also reported caveats to using a 2nd-degree polynomial, we opted to apply the 3rd-degree. For example, De Gier (2003) and Deo (2008) observed that in the scatter plot of tree AGB against DBH, the 2nd-degree curve fits extended below the *x*-axis at smaller tree diameters.

The rationale for this pixel-level curve fitting approach was to obtain a wall-to-wall inventory for any target year that did not have cloud-free satellite images. In addition, the fitted curves have the potential to minimize noise due to exogenous factors such as atmospheric influence. The curve-fit tool produced pixel-level model coefficients (as raster) that were used to obtain fitted predictors for all years in the recent cycle of NFI measurements (i.e., 2007–2011) and the other target years (i.e., 1990, 1995, 2000, and 2005). Thus, fitted predictors were obtained for each of the 5 years in the period 2007–2011. However, observed predictors were available for only 4 years in the same period (2007–2011) because a cloud-free Landsat image was not available in 2009. The fitted and observed predictors from 2007 to 2011 were next intersected with actual NFI plot locations of corresponding years to associate plot AGB with the predictors (i.e., no temporal mismatch). The spatial join was performed using ArcMap 10.2.[2] We attached the mean spectral values from each 3 × 3 pixel window to the measured plot response because the subplots in an NFI plot are distributed over nearly

[2] ESRI, Redlands, CA, USA, 2014.

a square block of nine 30-m by 30-m pixels. Hence, 2 training data frames, one with fitted and the other with observed metrics as predictors, were developed to formulate Landsat-dependent AGB models. Similarly, the LiDAR metrics and both observed and fitted Landsat predictors were attached to the AGB of NFI plots measured in 2011 to develop more training data frames for building LiDAR-dependent AGB models. We analyzed 2 types of LiDAR-dependent models, 1 using only LiDAR and the other using both LiDAR and Landsat variables (Table 4). In the following analysis, efforts were focused on identifying the most appropriate model for each of the reference (training) frames (Table 4).

The initial step in the process of model building was the identification and removal of multicollinear spatial predictors, as conducted in Falkowski et al. (2009), using a multivariate variable screening process based on QR-matrix decomposition (Cížková and Cížek 2012). We used a multicollinearity threshold value of 0.05 in this process, following Evans and Murphy (2015). We further leveraged a Random Forest (RF)-based model selection procedure (Falkowski et al. 2010; Murphy et al. 2010) to select an optimal RF model for predicting AGB for each reference frame (Figure 2). The RF model selection procedure[3] uses a percentage increase in model mean square error (MSE) to select a parsimonious RF model (fewest number of variables that explain the highest amount of variation) for predicting AGB.

The optimal models identified in the RF model selection procedure were then used in an RF-*k*NN imputation approach (Crookston and Finley 2008) to predict AGB. The imputation focused on spatially explicit prediction mapping of AGB based on the similarity of covariates at target and reference plots (pixels) where covariates were present at all target and reference points but the response observations were made only at the reference plots. Eighteen candidate models were evaluated; these models depended on different combinations of Landsat- and LiDAR-derived spatial predictors, number of observations used in the reference frame (i.e., plots within years), and number of nearest neighbors (i.e., value of k) considered for the imputation (Tables 4 and 5). We evaluated 3 values for k ($k = 1$, 3, and 5) in order to see the effect on accuracy and precision of the models. The models were first evaluated based on commonly used fit statistics (Heiskanen 2006), including the amount of variance explained, bias, and RMSE. Then the 6 models corresponding to an optimal value of k were extended spatially in 2011 (the only year for which LiDAR data were available). The 6 maps produced in 2011 were examined for accuracy, using the AGB data of 258 independent NFI plots measured in 2010. In addition, the map based on the best LiDAR-dependent model was considered as a reference and the other 5 models were evaluated by comparing the summaries of AGB predictions within 110 arbitrary polygons (~10 ha to 133 ha); these polygons were randomly shaped and sized and were obtained by digitizing forested areas on a false color composite of the Landsat image of 2011. The best-fit Landsat-based model was next extended temporally to the years 1990, 1995, 2000, 2005, and 2010. Accuracy of the model prediction was assessed in the year 2000 at the plot level by using the NFI plot data of 2000, and at the stand-level by comparing the aggregated pixel values of the 110 arbitrary polygons over forested areas against the corresponding estimates based on the NBCD map. The accuracy was assessed using the statistical measures of bias (observed–predicted), relative bias, RMSE, and relative RMSE as expressed by Heiskanen (2006).

[3] Available in the *rfUtilities* R package (Evans and Murphy 2015).

Results

Pixel-level curve fitting

Polynomial curve fitting to the time series of Landsat-derived 6 observed metrics resulted in a better coefficient of determination (R^2) (i.e., temporal consistency) with band-5 that produced R^2 values $\geq$ 0.40 in almost 50% of the total pixels in the target area. The polynomial fit to the observed time-series DI, IFZ, NBR, NDVI, and TCA metrics produced R^2 values $\geq$ 0.40 in 37.93%, 32.7%, 31.42%, 17.25% and 3.42% of the total pixels, respectively (Table 6). The texture of fitted metrics visually matched the corresponding observed metrics and false color composites of the Landsat image from the same date. For example, Figure 3 shows observed NDVI, fitted NDVI, and a false color composite of the Landsat image acquired on September 11, 2011.

Spatio-temporal inventory models

The multivariate variable screening for collinearity considerations and the RF-based model selection procedures revealed that all 6 Landsat-derived variables were important in those models dependent only on Landsat variables (i.e., all 6 Landsat predictors were selected). Figure 2 reveals the RF-based importance ranking of the predictors (Murphy et al. 2010) in the models corresponding to the 6 training data frames based only on Landsat variables and both LiDAR and Landsat variables combined (Table 4). In the combined Landsat and LiDAR-dependent model ($TM.LiDAR_{obs1}$), only 4 metrics, consisting of 3 LiDAR variables and Landsat Band 5 surface reflectance, were

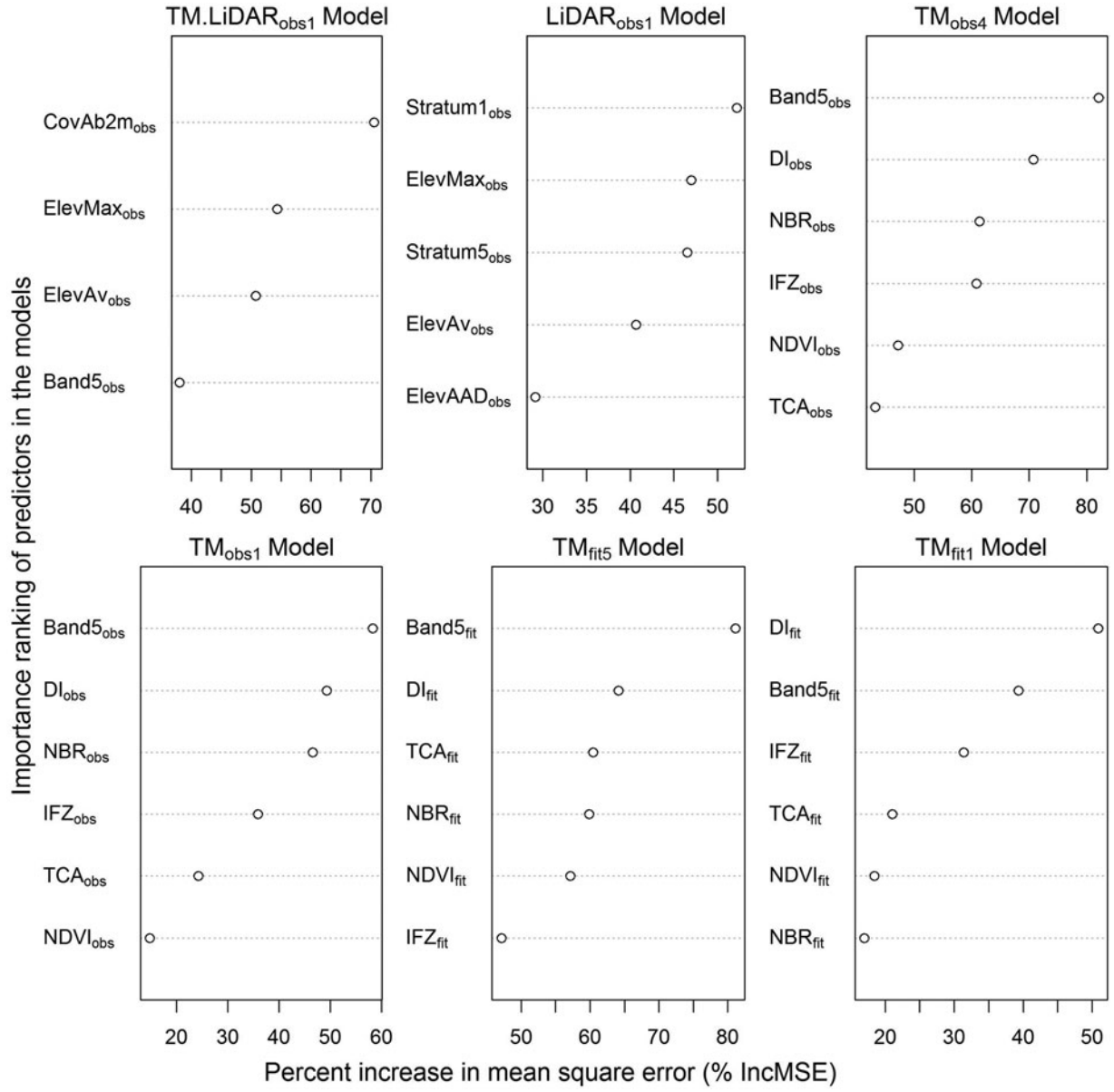

Figure 2. Random forest-derived importance ranking of the predictors used in the individual models. The ranking displays the most important variable at the top and the least important at the bottom for each model. Criterion for the ranking of variables was the percentage increase in model's mean square error when individual predictors are sequentially dropped and substituted with random numbers.

found to be useful for predicting AGB. The LiDAR metrics selected in the TM.LiDAR$_{obs1}$ model included average elevation (ElevAv) of pulse returns, maximum elevation (ElevMax), and cover estimate based on percentage of all returns above 2 m (CovAb2m). The LiDAR variables were the most influential in improving the model accuracy, compared to the Band 5 surface reflectance or other metrics derived from Landsat data. The model dependent only on LiDAR metrics (i.e., LiDAR$_{obs1}$ model, with no Landsat variables) selected 5 metrics, and the model produced accuracies close to but lower than those of the TM.LiDAR$_{obs1}$ model. Proportion of LiDAR returns below 1.5-m vertical height (Stratum1) and in the height interval from 10 m to 20 m (Stratum 5), average absolute deviations of elevations of the returns (ElevAAD), and the variables ElevMax and ElevAv were selected in the LiDAR$_{obs1}$ model (Table 4; Figure 2). The importance rankings of predictors were found to remain similar across the 3 k values (1, 3, and 5) in all the models. In the models dependent only on Landsat variables, Band 5 surface reflectance and DI consistently performed better than the other metrics of observed or fitted types.

The amount of variance explained and the other fit statistics (bias, relative bias, RMSE, and relative RMSE) for a model with a given training data frame were also found to be relatively stable with the 3 values of k (Table 5).

Table 5. Aboveground biomass models and its fit statistics for the various reference frames.

Model[†]	Value of *k*	% variance explained	Bias (Mg ha^{-1})	RMSE (Mg ha^{-1})	Relative bias %	Relative RMSE %
TM_{fit5}	1	25.79	1.06	48.69	1.36	62.32
TM_{fit1}	1	24.71	1.09	43.16	1.32	52.35
$TM.LiDAR_{obs1}$	1	62.82	1.17	30.42	1.43	35.96
$LiDAR_{obs1}$	1	60.59	1.58	32.64	1.94	40.23
TM_{obs4}	1	19.27	1.61	54.21	2.08	69.85
TM_{obs1}	1	24.64	−1.54	46.87	−1.81	55.09
TM_{fit5}	3	26.03	1.11	47.64	1.42	62.31
TM_{fit1}	3	24.88	0.47	42.16	0.56	50.76
$TM.LiDAR_{obs1}$	3	**62.86**	**0.40**	**27.20**	**0.48**	**34.76**
$LiDAR_{obs1}$	3	60.66	1.23	31.39	1.51	38.71
TM_{obs4}	3	18.95	1.32	54.18	1.69	69.53
TM_{obs1}	3	25.11	−1.73	46.70	−2.03	54.76
TM_{fit5}	5	25.87	1.18	48.51	1.51	62.19
TM_{fit1}	5	24.83	1.07	42.89	1.29	52.01
$TM.LiDAR_{obs1}$	5	62.80	1.08	29.05	1.32	35.59
$LiDAR_{obs1}$	5	60.53	1.26	31.53	1.55	38.73
TM_{obs4}	5	19.16	1.61	54.15	2.07	69.76
TM_{obs1}	5	24.67	−1.77	45.94	−2.07	53.85

[†] The numbers 4, 5, and 1 in the subscripts inform that the models included NFI plot data and corresponding spatial predictors from 4, 5, and 1 inventory years, respectively.

However, the $TM.LiDAR_{obs1}$ model explained the highest amount of variance followed by the $LiDAR_{obs1}$ model. The models dependent only on Landsat variables explained less than half of the total amount of variance explained by the LiDAR-dependent models (Table 5). A comparison of the imputed versus observed plot-level AGB by these models at $k = 1$ is shown in Figure 4. All the models produced positive bias (Table 5), except for the observed Landsat predictor-based model with fewer plots (TM_{obs1}), suggesting that the models led to under prediction of AGB. An assumption that the LiDAR-based models would be the most accurate is supported by the closer alignments of the 1:1 line with the linear fits between NFI plot observations in 2010 and the model predictions for the plots in 2011 (Figure 5, right). Pearson's correlation analysis of AGB observations at the NFI plots against predictions by the $TM.LiDAR_{obs1}$ and $LiDAR_{obs1}$ models at the same locations produced coefficients (r) of 0.7267 and 0.7086, respectively (Table 7a).

Although there was minimal difference in the values of model-fit statistics across the 3 levels of k, a value of $k = 3$ appeared to be optimal because it explained a larger amount of variance in 5 of the 6 models evaluated. The TM_{fit5} model explained the largest amount of variance after the 2 LiDAR-dependent models (Table 5); thus, the TM_{fit5} model was used to produce spatially explicit maps of AGB for the entire study area in the years 1990, 1995, 2000, 2005, 2010, and 2011. The 2 LiDAR-based models provided similar predictions to each other, and predictions by $TM.LiDAR_{obs1}$ model were closest to the 1:1 line (Figure 5). The plot-level predictions of the LiDAR-dependent models were closer to the predictions of observed Landsat-based models (TM_{obs}) than were the predictions of fitted Landsat-based models (TM_{fit}) (Table 7a). Similar trends were visible in the polygon-level total estimates of biomass by the models applied in 2011 (Figure 6; Table 8a). In terms of relative bias and RMSE of models dependent only on Landsat, the observed Landsat-based models performed better for plot (pixel)-level predictions (Table 7a) and fitted Landsat-based models performed better for the stand (polygon)-level predictions (Table 8a).

Plot-level validation of AGB predictions by the NBCD and TM_{fit5} models in 2000 using the NFI field observations for the same year revealed that the NBCD estimates provided better correlation than the estimates provided by the TM_{fit5} model (Figure 5; Table 7b). However, there was a very high correlation ($r = 0.9463$) between the

Table 6. Total number of pixels in the target area grouped into 5 classes based on pixel-level R^2 values of the polynomial curve fits to the time-series of individual metrics.

	Proportion of pixels (total: 21,382,738) in the classes of percentage R^2				
Metrics	0% – 20%	20% – 40%	40% – 60%	60% – 80%	80% – 100%
Band 5	22.28	27.00	23.76	19.54	7.42
DI	30.53	31.53	21.74	12.03	4.17
IFZ	35.06	32.24	20.02	10.18	2.50
NBR	34.72	33.86	20.59	8.81	2.02
NDVI	47.33	35.43	13.43	3.23	0.59
TCA	82.26	14.33	3.05	0.36	0.01

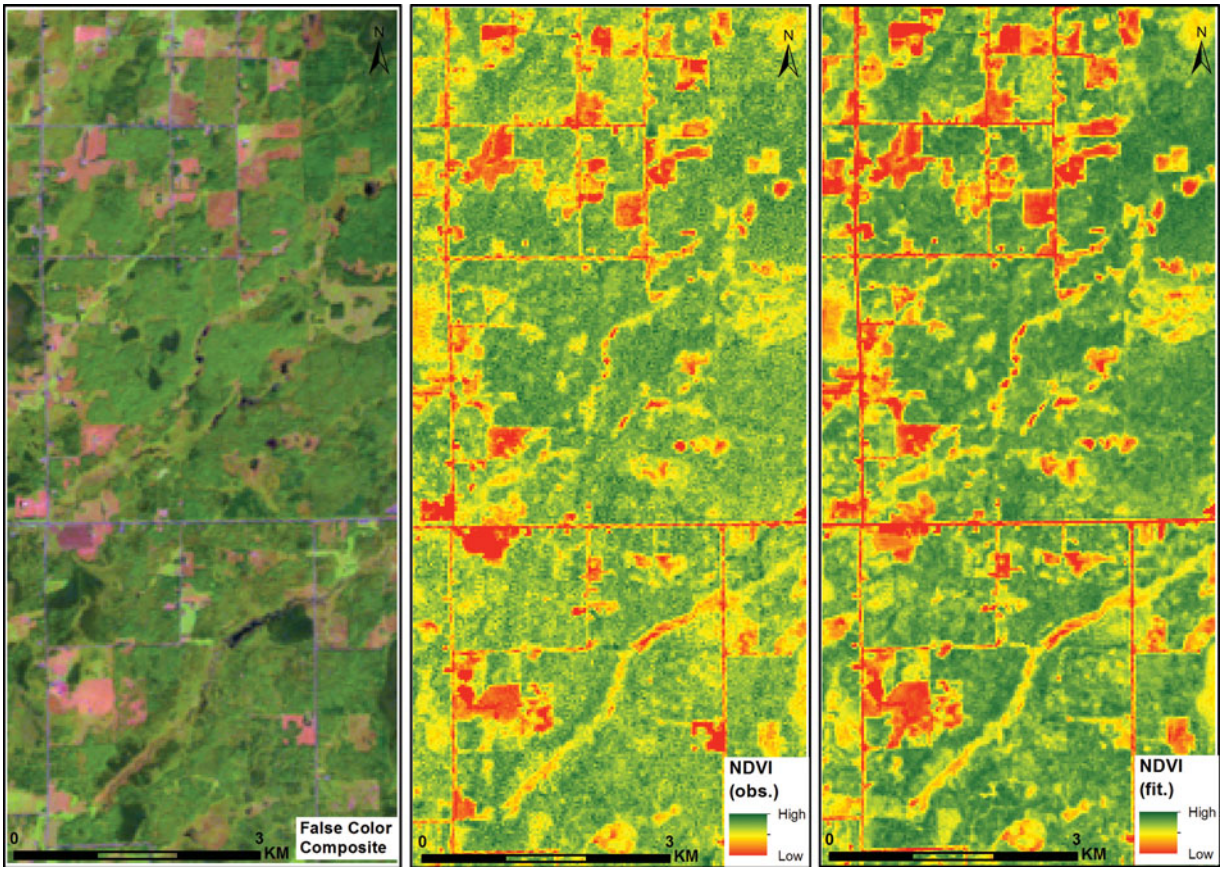

Figure 3. An image window (width 4,610 m; height 11,014 m) of Landsat TM data acquired on 11 September, 2011 over St. Louis county (Minnesota, U.S.A.) within the area of interest, displayed as a false color composite (TM bands 5, 4 and 1 represented as red, green and blue bands, respectively) to the left, observed NDVI in the middle and fitted NDVI (based on the polynomial fit) to the right. The red or pink tones are open canopy areas, black spots in the left panel are water bodies, and green areas are vegetation.

polygon-level estimates provided by the NBCD and TM_{fit5} models (Table 8b). An important result to notice from the plot-level validations is that NBCD estimates had a correlation coefficient of 0.6323 with the NFI field measurements of 2000, whereas estimates from the $TM.LiDAR_{obs1}$ model had a correlation coefficient of 0.7267 with the NFI field measurements of 2010. This implies that the LiDAR-based model was better than the NBCD model that used Radar-derived predictors. Therefore, the $TM.LiDAR_{obs1}$ model was used as a reference to evaluate polygon-level estimates of the other models in 2011 (Figure 6).

The spatially explicit mapping of AGB for the target years, based on the TM_{fit5} model, revealed biomass dynamics in the study area at 5-year intervals since 1990 (Table 9). The TM_{fit5} model provided an estimate of 137.85 ± 0.04 Tg in 2000 compared to 143.83 ± 0.03 Tg obtained from the NBCD 2000 map of the area. The same model produced 136.51 ± 0.04 Tg in 2011 compared to the 138.17 ± 0.04 Tg obtained from the $TM.LiDAR_{obs1}$

Table 7a Accuracy of the plot (pixel)-level aboveground biomass prediction estimates in 2011 for the 6 fitted models (at $k = 3$) validated with national forest inventory plot data measured in 2010.

	Plot-level validation with NFI data in 2010 ($n = 258$ plots)				
Model	r †	Bias (Mg ha^{-1})	RMSE (Mg ha^{-1})	Relative bias %	Relative RMSE %
TM_{fit5}	0.3436	3.17	54.19	4.23	72.29
TM_{fit1}	0.3507	4.08	54.39	5.45	72.56
$TM.LiDAR_{obs1}$	0.7267	2.75	38.57	3.68	51.46
$LiDAR_{obs1}$	0.7086	4.77	39.92	6.36	53.25
TM_{obs4}	0.4427	− 2.18	52.01	− 2.91	69.38
TM_{obs1}	0.4569	− 3.91	51.52	− 5.22	68.73

† Pearson's product-moment correlation.

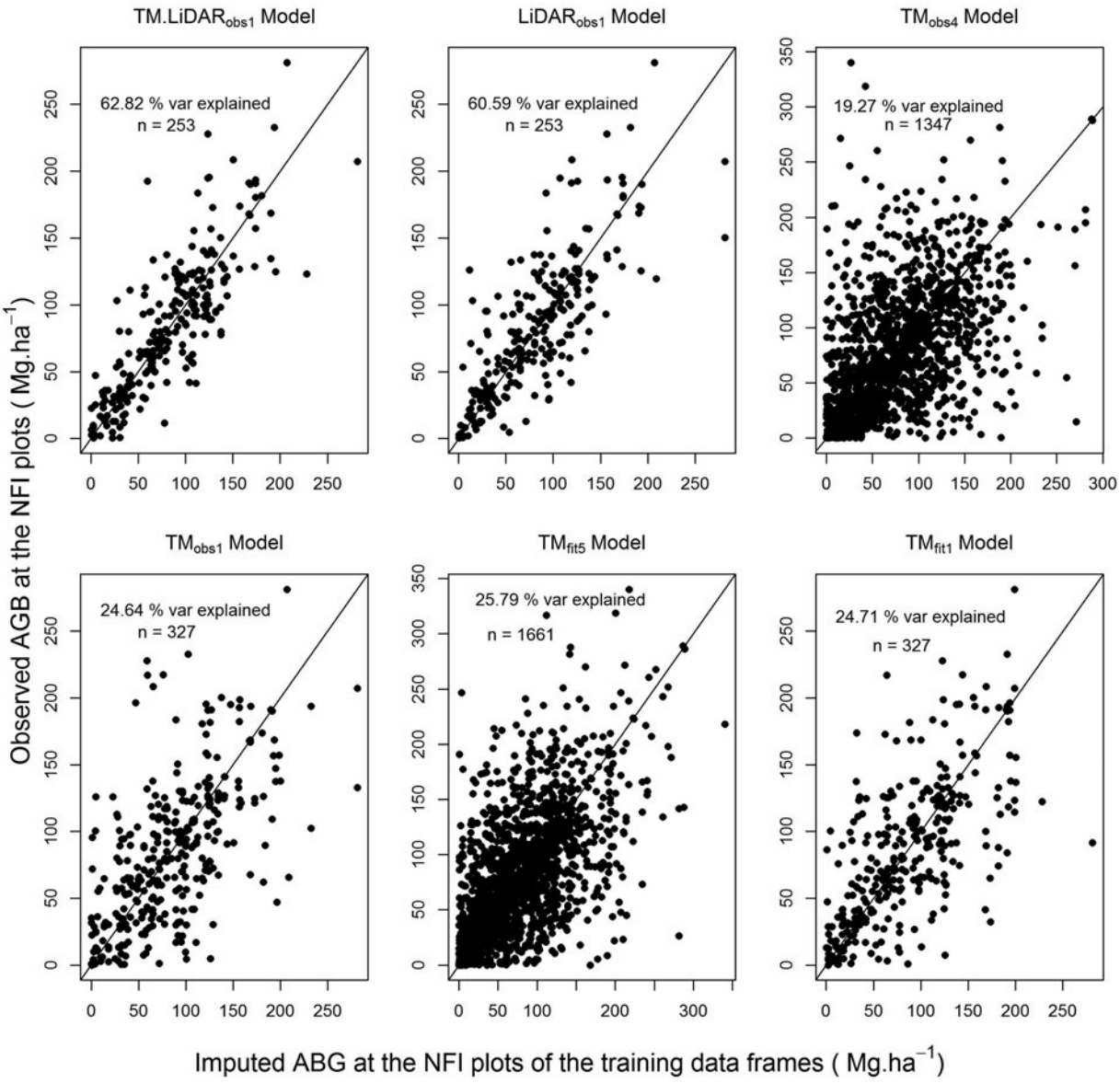

Figure 4. Plot-level imputed versus observed aboveground biomass (Mg ha^{-1}) by the six RF-*k*NN models (at $k = 1$) dependent either only on Landsat or both LiDAR and Landsat predictors in observed and fitted versions. These models predict aboveground biomass at a target plot from a nearest neighbor in the reference data frame and provide accuracy measures through internal cross-validation. The training sample size (n) of the models TM. LiDAR$_{obs1}$, LiDAR$_{obs1}$, TM$_{obs1}$, and TM$_{fit1}$ are small compared to TM$_{fit5}$ and TM$_{obs4}$ because the formers used inventory data of a single NFI panel (measurement year 2011) while TM$_{fit5}$ and TM$_{obs4}$ used data from five (2007-2011) and four (2007, 2008, 2010 and 2011) NFI panels, respectively. The inclined black lines are 1:1 lines.

model. The 1990 baseline estimate was found to be 142.79 ± 0.04 Tg for the area. A difference map of AGB predictions in 1990 and 2010 displayed a logical pattern with biomass losses in southwestern and some northern parts of the study area where there were higher human influences (Figure 7). Approximately 30% of the target area incurred ≥ 10 Mg ha^{-1} AGB loss and 34% area had ≥ 10 Mg ha^{-1} AGB gain, whereas in about 35% of the area the change remained within ± 10 Mg ha^{-1} over the 20-year period from 1990 to 2010.

Discussion

Although the historic use of remote sensing tools within the US NGHGI have mostly emphasized designation of forest/nonforest areas and poststratification for population estimates, the research presented herein highlights the efficacy of using Landsat time-series and LiDAR to inform and refine forest biomass baselines. Pixel-level model (polynomial) fitting to the dense temporal Landsat data can enhance AGB prediction accuracy to baseline years because the noise (due to factors such as sun angle,

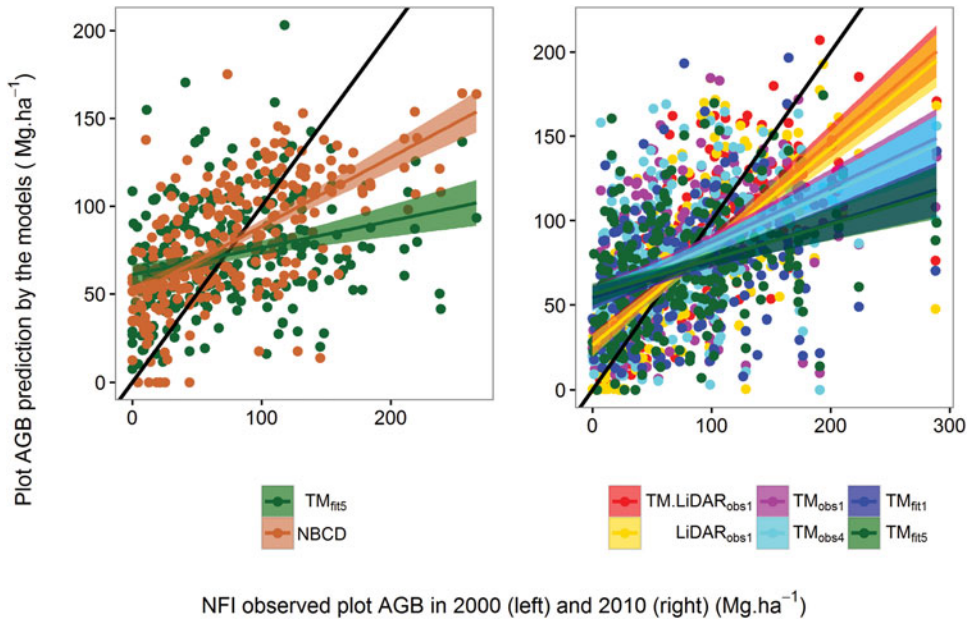

Figure 5. The cross validation of observed versus predicted NFI plot-level aboveground biomass in 2000 (left) and 2010 (right). The validation in the right is based on the field measurements of 2010 and predictions obtained for 2011. The dark inclined lines are the 1:1 lines and the color bands are the 95% confidence intervals for the linear fits. The models were based on $k = 3$.

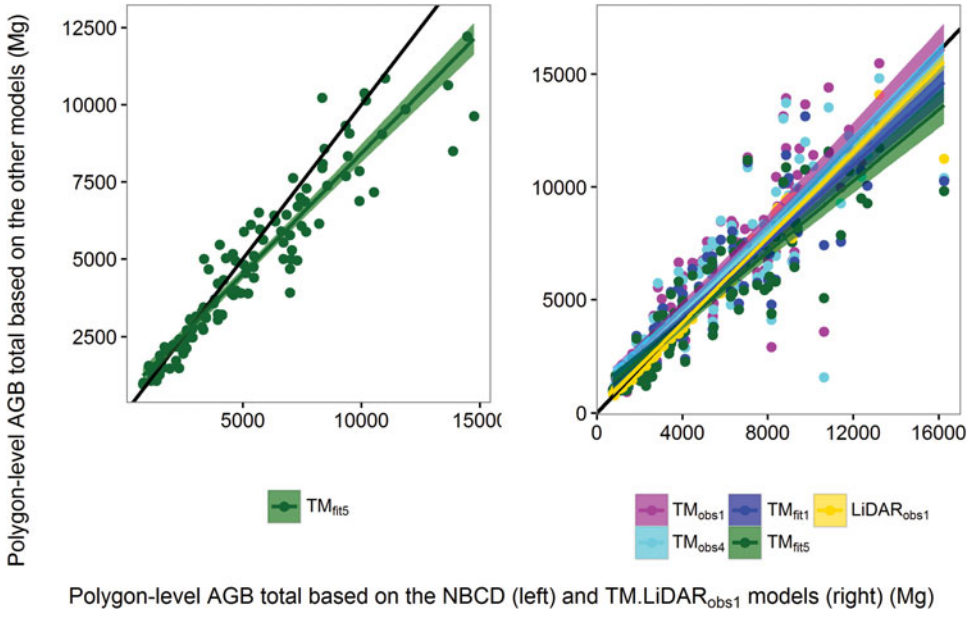

Figure 6. The cross validation of observed versus predicted polygon (stand)-level total aboveground biomass in 2000 (left) and 2010 (right). The validation in the left is based on the comparison of TM$_{fit5}$ model against the NBCD map of 2000, while validation in the right is based on the comparison of TM.LiDAR$_{obs1}$ model (i.e., using observed metrics of both Landsat and LiDAR) against all other models developed in 2011. The dark inclined lines are the 1:1 lines and the color bands are the 95% confidence intervals for the linear fits. The models were based on $k = 3$.

Table 7b. Accuracy of the plot (pixel)-level aboveground biomass predictions in 2000 by the TM$_{fit5}$ model (at $k = 3$) validated with national forest inventory plot data of the same year.

	Plot-level validation with NFI data in 2000 ($n = 270$)				
Model	r	Bias (Mg ha^{-1})	RMSE (Mg ha^{-1})	Relative bias %	Relative RMSE %
TM$_{fit5}$	0.2724	1.79	56.23	2.41	75.89
NBCD	0.6323	− 4.21	43.53	− 5.69	58.75

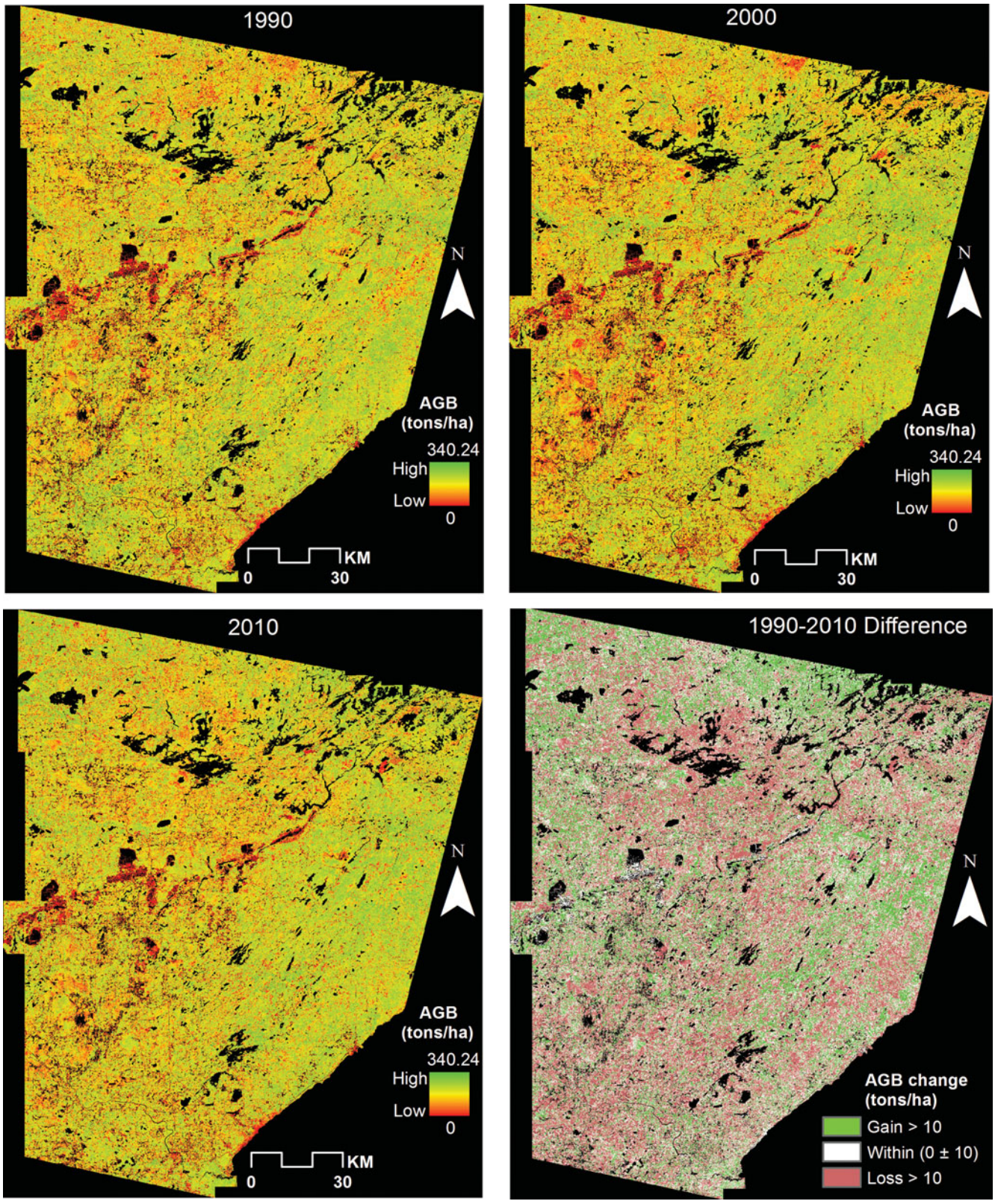

Figure 7. Projected aboveground biomass maps based on the TM_{fit5} model for the study area (north-eastern Minnesota, U.S.A.) in 1990 (top-left), 2000 (top-right) and 2010 (bottom-left), and the difference of AGB predictions in 1990 and 2010 (bottom-right).

Table 8a. Accuracy of polygon (stand)-level aboveground biomass prediction estimates in 2011 by the 5 fitted models (at $k = 3$) validated with the combined Landsat and LiDAR-based model ($TM.LiDAR_{obs1}$) estimates in the same year.

	Polygon-level validation with the $TM.LiDAR_{obs1}$ model based estimates in 2011 ($n = 110$ polygons)				
Model	r	Bias (Mg ha^{-1})	RMSE (Mg ha^{-1})	Relative bias %	Relative RMSE %
TM_{fit5}	0.9010	4.91	24.79	5.70	28.81
TM_{fit1}	0.9101	0.96	23.28	1.11	27.05
$LiDAR_{obs1}$	0.9867	1.60	9.35	1.85	10.86
TM_{obs4}	0.8733	− 4.46	28.88	− 5.18	33.55
TM_{obs1}	0.8783	− 8.54	30.09	− 9.92	34.96

Table 8b. Accuracy of the polygon (stand)-level prediction estimates in 2000 by the TM_{fit5} model (at $k = 3$) validated with the NBCD model estimates in the same year.

	Polygon-level validation with NBCD model estimate in 2000 ($n = 110$ polygons)				
Model	r	Bias (Mg ha^{-1})	RMSE (Mg ha^{-1})	Relative bias %	Relative RMSE %
TM_{fit5}	0.9463	8.91	21.13	10.26	24.33

Table 9 Total aboveground biomass in the study area (northeastern Minnesota, USA) for the baseline and other target years.

Year	Total [†] AGB (Tg)	Confidence interval of total AGB (Tg)	Standard deviation of pixel-level distribution in the maps (Mg ha^{-1})	Mean of pixel-level distribution in the maps (Mg ha^{-1})
1990	142.7945	± 0.0454	54.6302	74.2005
1995	152.2141	± 0.0486	58.4035	79.0952
2000	137.8553	± 0.0447	53.7626	71.6340
2005	157.4353	± 0.0482	57.9435	81.8084
2010	136.9765	± 0.0443	53.3184	71.1773
2011	136.5105	± 0.0442	53.1773	70.9352

[†] 1 Teragram (Tg) = 10^6 metric tons.

phenology, atmosphere, and sensor degradation) of predictor metrics are rectified in the process. In contrast to a single-date image snapshot, the temporal model fitting captures abrupt spectral changes in forested pixels (e.g., due to harvesting or fire) as well as slow regrowth processes following disturbance. This approach allows a more consistent trend analysis of forest biomass stocks after accounting for disturbances and regrowth while rectifying the inconsistencies in biomass and carbon accounting that result from changes in forest inventory protocols over time. In future NGHGIs, the approaches outlined here may inform forest biomass predictions in areas with few field observations from NFIs (e.g., interior Alaska in the U.S.A.).

The top-down approach of integrating remote sensing data with a sparse network of field-sample-plot data for large scale biomass mapping has shown varying degrees of success in published studies (Hall et al. 2006; Zheng et al. 2004). The accuracy in previous studies is found to be dependent on the quality of remote sensing (e.g., resolution and sensitivity to forest structure) and field data, as well as the choice of models and statistical indicators (Hayashi et al. 2015; Powell et al. 2010). Although Landsat-based models are traditionally formulated by using band reflectance and derived vegetation indices (Cohen and Goward 2004), selection of model type and predictors vary among studies and there is no generalized approach equally applicable across a range of forest conditions (Lu 2006). For example, Hall et al. (2006) used Landsat ETM+ visible and SWIR bands to model AGB. Jakubauskas (1996) and Lymburner et al. (2000) found that Landsat SWIR bands explained the most variation in forest structure. Jakubauskas and Prince (1997) observed statistically significant relationships for biomass dependent on Landsat Band 7 (i.e., midinfrared, $R^2 = 0.58$) and NDVI ($R^2 = 0.59$) for lodgepole pine forests in Yellowstone Park. Steininger (2000) found that Landsat Band 5 (i.e., SWIR) was the most important for modeling stand basal area and biomass in Brazil. Labrecque et al. (2006) found that Landsat Band 5 and tasseled cap indices resulted in maximum correlation to AGB compared to others indices such as NDVI, NBR, and band ratios. Foody et al. (2003) found that models with individual Landsat bands generally explained more variation in tropical forest biomass compared to derived vegetation indices. However, using derived spectral indices and biophysical variables in addition to untransformed Landsat band reflectances have improved biomass predictions in some studies (Powell et al. 2010; Hall et al. 2006). Our finding that Band 5 was the most influential predictor (Figure 2) in the Landsat-based models confirms this. This is not surprising, because empirical relationships

of remote sensing and forest biomass rely on the choice of model type, the forest type under study, and available variables for parameterization in addition to the effects of exogenous factors not related to any inherent relationship between spectral response and AGB. Some of the reported indices can also be obtained from Landsat MSS data, which has been available since 1972, and it is worth considering those metrics in future analyses when projecting AGB baselines beyond 1990 and after 1972.

In RF-*k*NN modeling, different values of k have been applied in different studies and are assumed to vary with sample size (Finley and McRoberts 2008; Franco-Lopez et al. 2001). For example, Falkowski et al. (2010) and Latifi et al. (2010) used $k = 1$ to predict different inventory attributes. Labrecque et al. (2006) used 5 neighbors ($k = 5$) in a k-NN imputation of biomass at pixel-level and found accuracies similar to a multiple linear regression approach. Powell et al. (2010) used a single neighbor in an imputation model (i.e., RF-based) for biomass and observed better performance with respect to other methods (e.g., reduced major axis regression). Tuominen and Pekkarinen (2005) tested 3 to 5 neighbors in the imputation of standing volume and found that $k = 5$ yielded the best estimation accuracy. Vauhkonen et al. (2010) proposed 2 to 4 neighbors, based on their results. Although some published works show that the estimation accuracy improves with increasing value of k (Tokola et al. 1996), higher values of k result in more smoothing of predictions. That said, a lower value of k is preferable in order to retain the variance structure of predictions closer to observations. The least amount of model bias and error in our analysis with $k = 3$ is in line with previous studies and supports a general guideline that a k value of 3 to 5 can be applied in the geospatial modeling of biomass.

The Landsat-based prediction estimates of plot-level AGB are satisfactory compared to published studies. We found RMSE in the range of 51.52 to 56.23 Mg ha^{-1} for the TM_{fit5} model (at $k = 3$) when validated with the NFI plot observations in the years 2000 and 2010 (Tables 7a and 7b). Powell et al. (2010) obtained an RMSE of 39.23 Mg ha^{-1} for the same area in Minnesota, however, there was no temporal difference in the training and validation datasets and also no fitting of predictors. Hall et al. (2006) reported RMSE of 33.7 Mg ha^{-1}–52.7 Mg ha^{-1} in Alberta, Canada, for different model forms dependent on Landsat ETM+ bands (3, 4, 5, and 7). Similarly, using raw Landsat bands and derived vegetation indices, Labrecque et al. (2006) obtained RMSE of 37 Mg ha^{-1}–85 Mg ha^{-1} with different model types in Newfoundland, Canada. In Wisconsin, using spectral bands (near-infrared and midinfrared) and vegetation indices, Zheng et al. (2004) found an RMSE of 54 Mg ha^{-1}. Huang et al. (2015) reported an RMSE of 58.2 Mg ha^{-1} when they validated their regional scale model in Maryland (also using a RF algorithm) based on LiDAR and high-resolution optical imagery. When they evaluated the NBCD product (at 30-m resolution) with NFI plot data in Maryland, they obtained an RMSE of 125.1 Mg ha^{-1}.

If we compare the plot-level bias and RMSE of the predictions by the TM_{fit5} model against the TM_{obs4} model, the latter have slightly lower error (Table 7a). But polygon-level predictions with the same models show similar bias and lower RMSE from the TM_{fit5} model (Table 8a). The marginally higher bias in plot (pixel)-level predictions with the TM_{fit5} model may be attributed to projection effects (i.e., alternations of observed Landsat signals in the metrics due to the polynomial fitting). It is important to note that all regional or national studies based only on Landsat data have reported issues with data saturation at high biomass levels. The positive biases in all model fits, except for the observed Landsat-based (TM_{obs1}) model, and in their pixel and polygon-level predictions indicate that the models produce underestimation particularly in high biomass areas, which is in concert with other findings such as Huang et al. (2015), Latifi et al. (2010), and Powell et al. (2014). The strength of our back-projection model (i.e., TM_{fit5}) is defensible because polygon-level predictions in 2000 have a high correlation with the NBCD estimates in the same year. Similarly, the predictions in 2011 have high correlations with $TM.LiDAR_{obs1}$ model-based estimates. Because the plot-level validations of NBCD and $TM.LiDAR_{obs1}$ models favor the latter (former has $r = 0.6323$, and the latter has $r = 0.7267$) and all the models in this study were developed using the RF algorithms, it is reasonable to conclude that the back-projection model is robust.

Although the model using both LiDAR and Landsat predictors explained more than 62% of the variance in the year of LiDAR acquisition, the model's strength may have degraded due to the extended period of LiDAR acquisition over 3 to 4 weeks in May with both leaf-off and leaf-on conditions. Although LiDAR underestimates canopy height in leaf-off conditions (due to fewer interceptions of pulses by canopy elements), and Landsat bands are subject to different reflectance properties (e.g., midinfrared bands are absorbed by leaf-water) in leaf-on and leaf-off seasons, the 2 types of remotely sensed data are likely to provide different structural information on forest attributes in the 2 different conditions. One fundamental reason is that the Landsat sensor can see only the extent of tree canopy (e.g., not DBH) and the cover estimate in leaf-off periods would be much less, compared to leaf-on periods. We can expect improved model accuracy when LiDAR data acquired at a time with uniform canopy conditions are integrated with

temporally matching Landsat data. The higher accuracy of the $TM.LiDAR_{obs1}$ model can be explained by the fact that Landsat data provide better estimates of canopy cover and LiDAR data provide accurate information on canopy height.

Forest canopy cover is one of the commonly used predictors in biomass modeling (Koch 2010). Pflugmacher et al. (2014) found LiDAR-derived mean canopy height and cover to be influential predictors that explained a large amount of variance (about 87%) in measured live tree biomass. Deo et al. (2016) and Takagi et al. (2015) also observed that LiDAR-derived mean canopy height explained a large amount of variance in plot AGB (>70%). The LiDAR metrics selected in our study were similar to these and other published works. However, it is commonly agreed that the predictive power of LiDAR metrics is affected by a number of factors such as sensor characteristics, season of acquisition, terrain form, forest types, crown composition, and data postprocessing steps. Model selection for a large area that includes different ecological sites is also challenging when training datasets do not sufficiently capture the variability in forest structures. The predictor variables found suitable in this study may or may not be appropriate in other areas.

Conclusions

The time-series Landsat data and the regional LiDAR dataset for the study area provided an excellent opportunity to evaluate the utility of optical remote sensing in characterizing aboveground forest biomass dynamics to inform spatially explicit baselines in the past when NFI data are limited. This work presents a realistic and consistent approach to support the US NGHGI and inform the 1990-baseline of AGB (or carbon stocks) and periodic stock changes thereafter per UNFCCC reporting requirements. The Landsat-based spatiotemporal model provided large-area AGB prediction accuracies comparable to an extant model (i.e., NBCD). The model using both LiDAR and Landsat-derived metrics was better for predicting AGB in the year of LiDAR acquisition than the model dependent only on LiDAR metrics. The number of explained variances and RMSEs of the $TM.LIDAR_{obs1}$, $LiDAR_{obs1}$, and TM_{fit5} models were 62.86%, 60.66%, and 26.03%, and 27.20 Mg ha^{-1}, 31.39 Mg ha^{-1}, and 47.64 Mg ha^{-1}, respectively (at $k = 3$). For polygon or stand-level estimation, the model dependent on fitted Landsat metrics performed better than the model based on observed metrics of the Landsat data. Hence, fitted Landsat metrics can be used in AGB modeling and mapping because the model improved accuracy for large-area estimation and further overcomes the challenge of obtaining cloud-free satellite images for a past target year. Because the observed LiDAR metrics compared to Landsat metrics significantly improved model accuracy in the year of LiDAR acquisition, further research is warranted to explore the potential of integrating high-quality LiDAR datasets (e.g., high point density) in back-projection modeling of AGB.

Acknowledgments

We thank Brian Clough, Jennifer Corcoran, John Stanovick, Ethan Butler, the Associate Editor, and two external reviewers for their comments that improved this work.

Funding

This work was supported by the USDA Forest Service, Northern Research Station and Minnesota Agricultural Experiment Station (project MIN-42-063).

References

Banskota, A., Kayastha, N., Falkowski, M.J., Wulder, M.A., Froese, R.E., and White, J.C. 2014. "Forest monitoring using landsat time series data: a review." *Canadian Journal of Remote Sensing*, Vol. 40(No. 5): pp. 362–384.

Brosofske, K., Froese, R.E., Falkowski, M.J., and Banskota, A. 2014. "A review of methods for mapping and prediction of inventory attributes for operational forest management." *Forest Science*, Vol. 60(No. 2): pp. 1–24.

Bechtold, W.A., and Scott, C.T. 2005. "The forest inventory and analysis plot design." General Technical Report SRS–GTR–80. In *The Enhanced Forest Inventory and Analysis Program–National Sampling Design and Estimation Procedures*, edited by W.A. Bechtold, and P.L. Patterson. Asheville, NC: USDA Forest Service, Southern Research Station.

Cížková, L., and Cížek, P. 2012. "Numerical linear algebra." In *Handbook of Computational Statistics: Concepts and Methods*, edited by J.E. Gentle, W.K. Hardle, and Y. Mori. Heidelberg: Springer.

Cohen, W.B., and Goward, S.N. 2004. "Landsat's role in ecological applications of remote sensing." *BioScience*, Vol. 54(No. 6): pp. 535–545.

Crist, E.P., and Cicone, R.C. 1984. "A physically based transformation of Thematic Mapper data – The TM Tasseled Cap." *IEEE Transactions on Geoscience and Remote Sensing*, Vol. GE–22(No. 3): pp. 256–263.

Crookston, N.L., and Finley, A.O. 2008. "yaImpute: an R package for kNN imputation." *Journal of Statistical Software*, Vol. 23(No. 10): pp. 1–16.

De Gier, A. 2003. "A new approach to woody biomass assessment in woodlands and shrublands." In *Geoinformatics for Tropical Ecosystems*, edited by P.S. Roy, pp. 161–198. Dehra Dun, India: Bishen Singh Mahendra Pal Singh.

De Jager, N.R., and Fox, T.J. 2013. "Curve fit: a pixel-level raster regression tool for mapping spatial patterns." *Methods in Ecology and Evolution*, Vol. 4(No. 8): pp. 789–792.

Deo, R.K. 2008. *Modeling and Mapping of Aboveground Biomass and Carbon Sequestration in The Cool Temperate Forest of North-East China*. Enschede, The Netherlands: ITC. accessed June 10, 2016, https://www.tc.nl/ilibrary/papers_2008/msc/nrm/deo.pdf

Deo, R.K., Froese, R.E., Falkowski, M.J., and Hudak, A.T. 2016. "Optimizing variable radius plot size and LiDAR resolution to model standing volume in conifer forests." *Canadian Journal of Remote Sensing*, Vol. 42(No. 5): pp. 428–442. doi: 10.1080/07038992.2016.1220826

Evans, J.S., and Murphy, M.A. 2015. *rfUtilities: random forests model selection and performance evaluation*. R package version 1.0–2, accessed November 10, 2015, http://cran.r–project.org/pack–age=rfUtilities

Escuin, S., Navarro, R., and Fernandez, P. 2008. "Fire severity assessment by using NBR (Normalized Burn Ratio) and NDVI (Normalized Difference Vegetation Index) derived from LANDSAT TM/ETM images." *International Journal of Remote Sensing*, Vol. 29(No. 4): pp. 1053–1073.

Falkowski, M.J., Evans, J.S., Martinuzzi, S., Gessler, P.E., and Hudak, A.T. 2009. "Characterizing forest succession with LiDAR data: an evaluation for the inland northwest, U.S.A." *Remote Sensing of Environment*, Vol. 113(No. 5): pp. 946–956.

Falkowski, M.J., Hudak, A.T., Crookston, N.L., Gessler, P.E., Uebler, E.H., and Smith, M.S. 2010. "Landscape–scale parameterization of a tree-level forest growth model: a k-nearest neighbor imputation approach incorporating LiDAR data." *Canadian Journal of Forest Research*, Vol. 40(No. 2): pp. 184–199.

Finley, A.O., and McRoberts, R.E. 2008. "Efficient k-nearest neighbor searches for multi–source forest attribute mapping." *Remote Sensing of Environment*, Vol. 112(No. 5): pp. 2203–2211.

Foody, G.M., Boyd, D.S., and Cutler, M.E.J. 2003. "Predictive relations of tropical forest biomass from Landsat TM data and their transferability between regions." *Remote Sensing of Environment*, Vol. 85(No. 4): pp. 463–474.

Franco-Lopez, H., Ek, A.R., and Bauer, M.E. 2001. "Estimation and mapping of forest stand density, volume, and cover type using the *k*–nearest neighbors method." *Remote Sensing of Environment*, Vol. 77(No. 3): pp. 251–274.

Gleason, C.J., and Im, J. 2011. "A review of remote sensing of forest biomass and biofuel: options for small-area applications." *GIScience & Remote Sensing*, Vol. 48(No. 2): pp. 141–170.

Goeking, S.A. 2015. "Disentangling forest change from forest inventory change: a case study from the US interior west." *Journal of Forestry*, Vol. 113(No. 5): pp. 475–483.

Hall, R.J., Skakun, R.S., Arsenault, E.J., and Case, B.S. 2006. "Modeling forest stand structure attributes using Landsat ETM+ data: application to mapping of aboveground biomass and stand volume." *Forest Ecology and Management*, Vol. 225(No. 1–3): pp. 378–390.

Hayashi, R., Kershaw, J.A., and Weiskittel, A. 2015. "Evaluation of alternative methods for using LiDAR to predict aboveground biomass in mixed species and structurally complex forests in northeastern North America." *Mathematical and Computational Forestry & Natural-Resource Sciences*, Vol. 7(No. 2): pp. 49–65.

Healey, S.P., Cohen, W.B., Zhiqiang, Y., and Krankina, O.N. 2005. "Comparison of tasseled cap-based landsat data structures for use in forest disturbance detection." *Remote Sensing of Environment*, Vol. 97(No. 3): pp. 301–310.

Heiskanen, J. 2006. "Estimating aboveground tree biomass and leaf area index in a mountain birch forest using ASTER satellite data." *International Journal of Remote Sensing*, Vol. 27(No.): 6, pp. 1135–1158.

Houghton, R.A., Hall, F.G., and Goetz, S.J. 2009. "Importance of biomass in the global carbon cycle." *Journal of Geophysical Research*, Vol. 114(No. G2): pp. 1–13.

Huang, C., Goward, S.N., Masek, J.G., Thomas, N., Zhu, Z., and Vogelmann, J.E. 2010. "An automated approach for reconstructing recent forest disturbance history using dense Landsat time series stacks." *Remote Sensing of Environment*, Vol. 114(No. 1): pp. 183–198.

Huang, W., Swatantran, A., Johnson, K., Duncanson, L., Tang, H., Dunne, J.O.N., et al. 2015. "Local discrepancies in continental scale biomass maps: a case study over forested and non-forested landscapes in Maryland, USA." *Carbon Balance and Management*, Vol. 10(No. 1): pp. 1–16.

Hudak, A.T., Crookston, N.L., Evans, J.S., Hall, D.E., and Falkowski, M.J. 2008. "Nearest neighbor imputation of species-level, plot-scale forest structure attributes from LiDAR data." *Remote Sensing of Environment*, Vol. 112(No. 5): pp. 2232–2245.

Hudak, A.T., Evans, J.S., and Smith, A.M.S. 2009. "LiDAR utility for natural resource managers." *Remote Sensing*, Vol. 1(No. 4): pp. 934–951.

Huete, A., Didan, K., Miura, T., Rodriguez, E.P., Gao, X., and Ferreira, L.G. 2002. "Overview of the radiometric and biophysical performance of the MODIS vegetation indices." *Remote Sensing of Environment*, Vol. 83(No. 1–2): pp. 195–231.

Huete, A., Miura, T., Yoshioka, H., Ratana, P., and Broich, M. 2014. "Indices of vegetation activity." In *Biophysical Applications of Satellite Remote Sensing*, edited by J.M. Hanes. Verlag Berlin, Heidelberg: Springer.

Hummel, S., Hudak, A.T., Uebler, E.H., Falkowski, M.J., and Megown, K.A. 2011. "A comparision of accuracy and cost of LiDAR versus stand exam data for landscape management of the Malheur national forest." *Journal of Forestry*, Vol. 109(No. 5): pp. 267–273.

Jakubauskas, M.E. 1996. "Thematic mapper characterization of lodgepole pine seral stages in Yellowstone National Park, USA." *Remote Sensing of Environment*, Vol. 56(No. 2): pp. 118–132.

Jakubauskas, M.E., and Price, K.P. 1997. "Empirical relationships between structural and spectral factors of Yellowstone lodgepole pine forests." *Photogrammetric Engineering and Remote Sensing*, Vol. 63(No. 12): pp. 1375–1381.

Jenkins, J.C., Chojnacky, D.C., Heath, L.S., and Birdsey, R.A. 2003. "National-scale biomass estimators for United States tree species." *Forest Science*, Vol. 49(No. 1): pp. 12–35.

Kellndorfer, J., Walker, W., Kirsch, K., Fiske, G., Bishop, J., LaPoint, L., et al. 2013. *NCAP Aboveground Biomass and Carbon Baseline Data (NBCD), U.S.A., 2000*. TN: Oak Ridge National Laboratory Distributed Active Archieve Center (ORNL DAAC), accessed May 14, 2016, http://dx.doi.org/10.3334/ORNLDAAC/1161

Kennedy, R.E., Yang, Z., and Cohen, W.B. 2010. "Detecting trends in forest disturbance and recovery using yearly Landsat time series: 1. LandTrendr–Temporal segmentation

algorithms." *Remote Sensing of Environment*, Vol. 114(No. 12): pp. 2897–2910.

Koch, B. 2010. "Status and future of laser scanning, synthetic aperture radar and hyperspectral remote sensing data for forest biomass assessment." *Journal of Photogrammetry and Remote Sensing*, Vol. 65(No. 6): pp. 581–590.

Labrecque, S., Fournier, R.A., Luther, J.E., and Piercey, D. 2006. "A comparison of four methods to map biomass from Landsat–TM and inventory data in western Newfoundland." *Forest Ecology and Management*, Vol. 226(No. 1–3): pp. 129–144.

Latifi, H., Nothdurft, A., and Koch, B. 2010. "Non-parametric prediction and mapping of standing timber volume and biomass in a temperate forest: application of multiple optical/LiDAR-derived predictors." *Forestry*, Vol. 839(No. 4): pp. 395–407.

Lawrence, R.L., and Ripple, W.J. 1999. "Calculating change curves for multitemporal satellite imagery: Mount St. Helens 1980–1995." *Remote Sensing of Environment*, Vol. 67(No. 3): pp. 309–319.

Liaw, L.A., and Wiener, M. 2002. "Classification and regression by random forest." *R News*, Vol. 2: pp. 18–22.

Lillesand, T.M., Kiefer, R.W., and Chipman, J.W. 2007. *Remote Sensing and Image Interpretation*, 6th *Edition*. Hoboken, NJ: John Wiley & Sons.

Lu, D. 2006. "The potential and challenge of remote sensing-based biomass estimation." *International Journal of Remote Sensing*, Vol. 27(No. 7): pp. 1297–1328.

Lu, D., Chen, Q., Wang, G., Moran, E., Batistella, M., Zhang, M., et al. 2012. "Aboveground forest biomass estimation with Landsat and LiDAR data and uncertainity analysis of the estimates." *International Journal of Forestry Research*, Vol. 2012(No. 436537): pp. 1–16.

Lymburner, L., Beggs, P., and Jacobson, C. 2000. "Estimation of canopy-average surface-specific leaf area using Landsat TM data." *Photogrammetric Engineering and Remote Sensing*, Vol. 66(No. 2): pp. 183–191.

McGaughey, R.J. 2014. *FUSION/LDV: Software for LiDAR Data Analysis and Visualization, Version 3.21*. Seattle, WA: USDA Forest Service, Pacific Northwest Research Station, University of Washington.

McRoberts, R.E. 2009. "Diagnostic tools for nearest neighbors techniques when used with satellite imagery." *Remote Sensing of Environment*, Vol. 113(No. 3): pp. 489–499.

McRoberts, R.E. 2012. "Estimating forest attribute parameters for small areas using nearest neighbors techniques." *Forest Ecology and Management*, Vol. 272(No. 15): pp. 3–12.

MN DNR. 2013. *Minnesota Facts and Figures*. Minnesota Climatology working group, Minnesota Department of Natural Resources, accessed April 12, 2013, http://www.dnr.state.mn.us/–faq/mnfacts/climate.html

MnGeo. 2015a. *LiDAR Elevation, Arrowhead Region, NE Minnesota*. Minnesota Geospatial Information Office: Minnesota Department of Natural Resources, accessed December 17, 2015, http://www.mngeo.state.mn.us/chouse/metadata/lidar_arrowhead2011.html

MnGeo. 2015b. *LiDAR Elevation Data for Minnesota*. Minnesota Geospatial Information Office, Minnesota Department of Natural Resources, accessed December 17, 2015, http://www.mngeo.–state.mn.us/chouse/elevation/lidar.html#data

MnTOPO. 2014. *MnTOPO Help: Revolutionizing the Way We Look at Minnesota's Landscape*. Minnesota Department of Natural Resources, accessed December 17, 2015, http://files.dnr.–state.mn.us/aboutdnr/gis/mntopo/mntopo_help_document.pdf

Moser, P., Vibrans, A.C., McRoberts, R.E., Næsset, E., Gobakken, T., Chirici, G., et al. 2016. "Methods for variable selection in LiDAR-assisted forest inventories." *Forestry*, Vol. 89(No. 4): pp. 1–13. doi:10.1093/forestry/cpw041

Murphy, M.A., Evans, J.S., and Storfer, A. 2010. "Quantifying Bufo boreas connectivity in Yellowstone National Park with landscape genetics." *Ecology*, Vol. 91(No. 1): pp. 252–261.

Nabuurs, G.J., Masera, O., Andrasko, K., Benitezâ€"Ponce, P., Boer, R., Dutschke, M., et al. 2007. "Forestry." In *Climate Change Mitigation: Contribution of Working Group III to the Fourth Assessment Report of the Intergovernmental Panel on Climate Change*, edited by B. Metz, O. Davidson, P. Bosch, R. Dave, and L. Meyer. Cambridge, UK/New York, USA: Cambridge University Press.

Pan, Y., Birdsey, R.A., Phillips, O.L., and Jackson, R.B. 2013. "The structure, distribution, and biomass of the world's forests." *Annual Review of Ecology, Evolution, and Systematics*, Vol. 44: pp. 593–622.

Pflugmacher, D., Cohen, W.B., and Kennedy, R.E. 2012. "Using Landsat-derived disturbance history (1972–2010) to predict current forest structure." *Remote Sensing of Environment*, Vol. 122(Landsat legacy special issue): pp. 146–165.

Pflugmacher, D., Cohen, W.B., Kennedy, R.E., and Yang, Y. 2014. "Using Landsat-derived disturbance and recovery history and lidar to map forest biomass dynamics." *Remote Sensing of Environment*, Vol. 151(No. 2012 ForestSAT): pp. 124–137.

Powell, S.L., Cohen, W.B., Healey, S.P., Kennedy, R.E., Moisen, G.G., Pierce, K.B., et al. 2010. "Quantification of live aboveground forest biomass dynamics with Landsat time-series and field inventory data: a comparison of empirical modelling approaches." *Remote Sensing of Environment*, Vol. 114(No. 5): pp. 1053–1068.

Powell, S.L., Cohen, W.B., Kennedy, R.E., Healey, S.P., and Huang, C. 2014. "Observation of trends in biomass loss as a result of disturbance in the conterminous U.S.: 1986–2004." *Ecosystems*, Vol. 17(No. 1): pp. 142–157. doi: 10.1007/s10021-013-9713-9

R Core Team. 2015. *R: A Language and Environment for Statistical Computing*. Vienna, Austria: R Foundation for Statistical Computing, accessed Nov. 10, 2015, http://www.R-project.org/

Roy, D.P., Wulder, M.A., Loveland, T.R., Woodcock, C.E., Allen, R.G., Anderson, M.C., et al. 2014. "Landsat-8: science and product vision for terrestrial global change research." *Remote Sensing of Environment*, Vol. 145(No. 5): pp. 154–172.

Schroeder, T.A., Gray, A., Harmon, M.E., Wallin, D.O., and Cohen, W.B. 2008. "Estimating live forest carbon dynamics with a Landsat-based curve-fitting approach." *Journal of Applied Remote Sensing*, Vol. 2(No. 023519): pp. 1–20.

Steininger, M.K. 2000. "Satellite estimation of tropical secondary forest above-ground biomass: data from Brazil and Bolivia." *International Journal of Remote Sensing*, Vol. 21(No. 6–7): pp. 1139–1157.

Takagi, K., Yone, Y., Takahashi, H., Sakai, R., Hojyo, H., Kamiura, T., et al. 2015. "Forest biomass and volume estimation using airborne LiDAR in a cool-temperate forest of northern Hokkaido, Japan." *Ecological Informatics*, Vol. 26(No. 3): pp. 54–60.

Tokola, T., Pitkanen, J., Partinen, S., and Muinonen, E. 1996. "Point accuracy of a non-parametric method in estimation of forest characteristics with different satellite materials." *International Journal of Remote Sensing*, Vol. 17(No. 12): pp. 2333–2351.

Tomppo, E. 1991. "Satellite image based national forest inventory of Finland." *International Archives of Photogrammetry and Remote Sensing*, Vol. 27(No. 7.1): pp. 419–424.

Tuominen, S., and Pekkarinen, A. 2005. "Performance of different spectral and textural aerial photograph features in multi–source forest inventory." *Remote Sensing of Environment*, Vol. 94(No. 2): pp. 256–268.

USGS. 2015a. "Landsat 4–7 climate data record (CDR) surfance reflectance." *Department of Interior, U.S. Geological Survey. Product Guide Version 6.6*, accessed April 5, 2016, http://landsat.usgs.gov/documents/cdr_sr_product_guide.pdf

USGS. 2015b. "Earth resources observation and science (EROS) center science processing architecture (ESPA) on demand interface." *Department of Interiour, U.S. Geological Survey. Product Guide Version 3.2*, accessed April 5, 2016, http://landsat.usgs.gov/documents/espa_odi–_userguide.pdf

USGS. 2016. "Landsat surface reflectance-derived spectral indices." *U. S. Geological Survery Earth Resources Observation and Science Center. Product Guide Version 2.9*, accessed April 11, 2016, http://landsat.usgs.gov/documents/si_product_guide.pdf

Vauhkonen, J., Korpela, I., Maltamo, M., and Tokola, T. 2010. "Imputation of single-tree attributes using airborne laser scanning-based height, intensity, and alpha shape metrics." *Remote Sensing of Environment*, Vol. 114(No. 6): pp. 1263–1276.

Zhang, X., and Ni-Meister, W. 2014. "Remote sensing of forest biomass." In *Biophysical Applications of Satellite Remote Sensing*, edited by J.M. Hanes. Berlin, Heidelberg: Springer-Verlag.

Zheng, D., Rademacher, J., Chen, J., Crow, T., Bresee, M., Moine, J.L., and Ryu, S.R. 2004. "Estimating aboveground biomass using Landsat 7 ETM+ data across a managed landscape in northern Wisconsin, USA." *Remote Sensing of Environment*, Vol. 93(No. 3): pp. 402–411.